

1 **Assessment of vulnerability to erosion: digital mapping of a loess cover**  
2 **thickness and stiffness using spectral analysis of seismic surface-waves**

3  
4 *K. Samyn<sup>\*1</sup>, O. Cerdan<sup>1</sup>, G. Grandjean<sup>1</sup>, R. Cochery<sup>1</sup>, S. Bernardie<sup>1</sup>, A. Bitri<sup>1</sup>*

5  
6 *(1) BRGM, Risks Department, 3 Avenue Claude Guillemin, BP36009 45060 Orléans*  
7 *Cedex 2, France*

8  
9 *\* Corresponding author. BRGM, Risks Department, 3 Avenue Claude Guillemin*  
10 *BP36009 45060 Orléans Cedex 2, France. Tel.: +33 (0)2 38 64 34 54; fax: +33*  
11 *(0)2 38 64 36 89. E-mail address: k.samyn@brgm.fr (K. Samyn).*

12  
13 **Abstract**

14  
15 Non-invasive geophysical techniques offer an interesting alternative to  
16 traditional soil sampling methods, especially for estimating spatial variations of  
17 soil parameters in the landscape. The spectral analysis of seismic surface-  
18 waves (*MASW*) can be used to determine the vertical shear-wave velocity (*V<sub>s</sub>*)  
19 model (i.e., vertical variations in *V<sub>s</sub>* with depth). In our study, *MASW* soundings  
20 were determined at each point in a grid spread over a wind-eroded field plot of  
21 15600 m<sup>2</sup>. *V<sub>s</sub>* was then mapped in terms of the thickness and stiffness of the  
22 superficial loamy material horizon, which are called *ThickLM* and *StiffLM*,  
23 *respectively*. To relate the *V<sub>s</sub>* values to the soil stiffness, cone resistance (*Q<sub>d</sub>*)

24 soundings were also performed using a Dynamic PANDA penetrometer.  
25 Concurrently, boreholes were used to sample the same horizon for bulk soil  
26 density ( $\rho_b$ ) measurements. Based on these measurements, large variations in  
27 *ThickLM* were observed. The distribution of  $V_s$  values along a 130 m transect  
28 allowed for the distinction between two layers corresponding to different  
29 mechanical properties. The  $V_s$  value of 240 m/s was then used as a limit  
30 between the loamy material and the underlying clays. This limit was validated  
31 using drilling observations performed on the same transect. Therefore, it was  
32 possible to map the *ThickLM*, which varied between 0.2 and 6.5 m over the  
33 entire field. The comparison between the averaged values of  $V_s$  and  $Q_d$  in the  
34 loamy material layer showed a significant correlation ( $R^2=0.4$ ) such that the  
35 mapping of *StiffLM* was realised from the  $V_s$  map and the  $V_s$ - $Q_d$  relationship.  
36 Density comparison between the  $\rho_b$  measured on drill samples and the  $\rho_b$   
37 calculated from  $V_s$  were also performed using previously published  
38 relationships; however, significant correlations were not observed. The obtained  
39 maps of *ThickLM* and *StiffLM* were consistent with the expected effects of  
40 erosion at the catchment scale and provide indications of historical erosion  
41 events. This methodology, which provides a structural and mechanical  
42 characterisation of subsurface materials, should help to focus conservation  
43 measures to the most threatened areas (i.e., the identification of areas that  
44 show a reduced *ThickLM* and increased *StiffLM*, which are associated with high  
45 soil erosion vulnerability and/or high compaction state).

46

47 **Keywords**

48

49 Surface wave; Erosion; Digital mapping; Shear wave velocity; Cone resistance

50

51 **1. Introduction**

52

53 The current growing awareness of ecological issues has led to an increasing  
54 demand for environmental datasets that are necessary for adequate monitoring  
55 and management of various threatened ecosystems. There is also a growing  
56 concern regarding the sustainability of biomass production, not only in  
57 developing or semi-arid areas (Hadgu et al., 2009; Ye and Van Ranst, 2009) but  
58 also in industrialised countries. The increasing demand for cereals and biofuels  
59 will further accentuate this trend. Strong relationships between soil erosion, soil  
60 depth and soil productivity have been reported in various environments (e.g.,  
61 Biot and Lu, 1995; Tendberg et al., 1997; Heckrath et al., 2005; Rejman and  
62 Iglík, 2010). The regolith and, more generally, the soil surface material are  
63 particularly important, as they support human activities and fulfil numerous  
64 ecosystem services (European Commission., 2002-2006). However, our  
65 knowledge of the nature and spatial extent of surficial materials is far from  
66 complete, and therefore further research is necessary to fill this gap. The ability  
67 to accurately and rapidly produce soil depth maps or to delineate areas with

68 limited root penetration depths will, therefore, become crucial to address these  
69 issues. Conventional soil surveys are generally based on manual sampling and  
70 visual observations of soil pits or auger holes. Such observations are met with  
71 both methodological and economic constraints when used for the investigation  
72 of large areas. Not only are these observations extremely time consuming – and  
73 thus costly – because of the highly repetitive fieldwork that is needed, they can  
74 also be destructive to the soil. Moreover, this type of local observation may not  
75 represent larger-scale trends in soil properties.

76 Geophysical techniques offer an interesting alternative to traditional soil  
77 sampling methods, especially for estimating the spatial variability of physical soil  
78 parameters of large areas. These techniques are particularly relevant because  
79 most physical soil characteristics are closely related to soil properties (e.g., geo-  
80 electrical properties) (Rhoades and van Schilfgaarde, 1976; Robain et al., 1996;  
81 Samouëlian et al., 2005). For example, a significant correlation has been  
82 demonstrated between the apparent electrical resistivity ( $\rho$ ) or electrical  
83 conductivity ( $\sigma$ ) and the soil texture (Williams and Hoey, 1987), soil water  
84 content (Kachanoski et al., 1988; Kalinski and Kelly, 1993; Michot et al., 2003),  
85 soil salt or nutrient content (Rhoades and Corwin., 1981; Eigenberg et al., 1998)  
86 or soil depth (Thompson and Bell., 1996; Chaplot et al., 2001). In contrast to  
87 these electrical methods, seismic techniques are not well established in soil  
88 sciences but could be particularly promising. Due to the development of  
89 subsurface characterisation studies for environmental or geotechnical purposes,

90 the efficiency of seismic methods for estimating ground velocity structures and  
91 mechanical properties has seen considerable progress in the recent decades  
92 and has been used in various applications in several fields: waste disposal  
93 (Lanz et al., 1998), landslides (Grandjean et al., 2007), or hydrogeophysics  
94 (Sturtevant et al., 2004). Modern equipment, which generally features 48 or 72  
95 recording channels and PC-piloted acquisition software, has made this method  
96 user-friendly and has contributed to its popularity. Recently, an adaptation of the  
97 sensor line, which is based on unplugged gabled geophones, was proposed  
98 to drastically reduce the acquisition times (Grandjean, 2006a; Debeglia et al.,  
99 2006). This improvement was supported by the development of new data  
100 processing protocols, such as acoustical tomography (Azaria et al., 2003;  
101 Grandjean, 2006b) or spectral analysis of surface-waves (SASW) (Nazarian et  
102 al., 1983; Park et al., 2000; Grandjean and Bitri, 2006) and related multichannel  
103 MASW applications (Foti, 2000; Miller, 1999; Park et al., 1999a, 1999b; Xia et  
104 al., 1999), which allowed for the construction of shear waves velocity ( $V_s$ )  
105 profiles. For example, the analysis of fundamental-mode Rayleigh waves is one  
106 of the most common methods for using the dispersive properties of surface  
107 waves (Bullen, 1963). This type of analysis provides essential parameters that  
108 are commonly used to evaluate near-surface stiffness, which is a critical  
109 property for many geotechnical studies (Stokoe et al., 1994). SASW uses the  
110 spectral analysis of the ground roll that is generated by an impulsive source and  
111 is recorded by a pair of receivers. This method has been widely and effectively

112 used in many geotechnical engineering projects (Stokoe et al., 1994). A single  
113 pair of receivers is configured and reconfigured (based on wavelength  
114 calculations made during the acquisition) as many times as necessary to  
115 sample the desired frequency range. Unfortunately, the necessity of recording  
116 repeated shots during multiple field deployments for a given site increases the  
117 time and labour requirements relative to a multichannel procedure. Multichannel  
118 analysis of surface waves (MASW) is designed to overcome the few  
119 weaknesses of the SASW method. The purpose of this study is to test the  
120 MASW method as a new tool for characterising soil mechanical properties (i.e.,  
121 soil thickness and stiffness) with respect to erosion processes.

122 Instead of sounding the area by systematic drilling, seismic methods were  
123 tested to efficiently produce soil property maps. Specifically, we evaluated the  
124 feasibility of using mechanical contrasts that exist between the lithologies to  
125 map the thickness and stiffness (*ThickLM* and *StiffLM*, respectively) of the  
126 surface loamy material horizon using  $V_s$  data. Based on this process, we should  
127 be able to identify the most threatened areas at the catchment scale, i.e., areas  
128 that show a reduced *ThickLM* associated with high *StiffLM*, using  $V_s$  data  
129 coupled to cone resistance ( $Qd$ ) data because *StiffLM* can be used as a  
130 surrogate for the soil erodibility.

131

## 132 **2. Materials and methods**

133

134 2. 1. *Description of the study field*

135

136 The study area was located within the Bourville catchment in Normandy, a  
137 region of Northern France where erosion that removes the upper soil horizons is  
138 a major threat to the main soil functions (i.e., “food and other biomass  
139 production, storage, filtering, and transformation of elements among which  
140 water and nutrients, biological habitat, and source of raw materials”, European  
141 Commission, 2002; Van-Camp et al., 2004). The studied area includes a  
142 catchment of the European loess belt in Normandy; this region is severely  
143 affected by water and wind erosion with rates often exceeding soil production  
144 (between 5 and 10  $\text{ton}\cdot\text{ha}^{-1}\cdot\text{yr}^{-1}$ ; Cerdan et al., 2010) (Figure 1). Normandy has  
145 a humid-temperate climate with few days of frost. The average temperature  
146 ranges between 10 and 12 °C throughout the year, and in August, which is the  
147 hottest month of the year, the temperature fluctuates approximately 18 °C. The  
148 hilly areas, characterised by a smooth relief (0-7%) and deep superficial layer  
149 (>5 m), are used for intensive production of alternating winter and spring crops  
150 (e.g., wheat, beets, and maize). An area of approximately 1.5 ha was selected  
151 in this catchment to test our approach. Not only was this area highly degraded  
152 with a quasi-complete removal of the soil cover in certain areas, its surrounding  
153 areas also showed a gradation in the thickness of the loamy material horizon  
154 from thick and well conserved in the low elevation locales to thin and eroded in  
155 the high elevation areas. The research plot was delineated within the transition

156 zone. This plot, which extended along the steepest slope (Figure 1), shows  
157 clear evidence of soil degradation in its north-west and south-east areas with  
158 the presence of outcropping clays with flints, both of which are characteristics of  
159 on-going loamy material horizon erosion. The entire soil surface was covered by  
160 grass vegetation during the field study.

161

## 162 *2. 2. Geological setting and geomorphologic conditions*

163 The study area was located in north-western France (Normandy), which is  
164 characterised by a humid-temperate climate. The topography was relatively  
165 smooth with slope gradients ranging between 1% and 4% on the plateau and  
166 4% to 10% on valley sides. The area is covered by silt loam soils, which  
167 developed on the loess Quaternary deposit, and contains at least 60% silt in the  
168 surface horizons. These soils are classified as Neoluvisol in the French  
169 Classification system and are described as 'excessively drained' according to  
170 the USDA (2003) soil drainage classification (Orthic Luvisol, [World Reference](#)  
171 [Base, 1998](#)). Such soils are very sensitive to soil sealing because of their low  
172 clay content (130 to 170 g.kg<sup>-1</sup>) and low organic matter content (10 to 20 g.kg<sup>-1</sup>)  
173 relative to more competent underlying clays that are enriched with flints. When  
174 in arable use, large areas are left bare and open to rainfall during most of the  
175 cultural season, which, combined with the sensitivity to sealing, renders them  
176 vulnerable to runoff and water erosion (Figure 2). In contrast, sediments  
177 accumulate due to erosion flows in sheltered areas. Based on the

178 geomorphologic conditions, the thickness of the uppermost loamy sediments  
179 presents a high variability at the catchment scale.

180

### 181 *2. 3. Theory and basic principles of the MASW method*

182

183 In the majority of surface seismic surveys, when a compressional wave source  
184 is used, more than two-thirds of the total seismic energy generated is imparted  
185 into Rayleigh waves (Richart et al., 1970), which is the principal component of  
186 surface waves. Assuming vertical velocity variation, each frequency component  
187 of a surface wave has a different propagation velocity (called the phase velocity,  
188  $C_f$ ) at each unique frequency ( $f$ ) component. This unique characteristic results  
189 in a different wavelength ( $\lambda_f$ ) for each frequency that is propagated. This  
190 property is called dispersion. Although surface waves are considered noise in  
191 body-wave surveys (i.e., reflection or refraction profiling), their dispersive  
192 properties can be used to infer near-surface elastic properties via Vs evaluation  
193 (Nazarian et al., 1983; Stokoe et al., 1994; Park et al., 1998a). The entire  
194 process typically used to produce reliable Vs profiles via the spectral analysis of  
195 surface waves involves three steps: (1) the acquisition of surface waves (Figure  
196 3,5a), (2) the construction of dispersion curves (a plot of phase velocity as a  
197 function of  $f$ ) (Figure 5b), and (3) the back calculation (inversion) of the Vs  
198 profile from the calculated dispersion curve (Figure 5c,d). A workflow diagram

199 illustrating the processing method used to obtain reliable Vs profiles with depth  
200 is presented in Figure. 4.

201 For step (1), to obtain a good estimation of dispersion curves, we used a multi-  
202 station (MASW) configuration, in which receivers are set at several locations  
203 and are regularly spaced along a straight line. A seismic source signal was  
204 generated via the impact of a hand-held hammer hitting a small iron anvil  
205 located on the ground. During the recording, the wavefield was discretised and  
206 truncated in both the time and space domain (Figure 5a). The sampling periods  
207 in the time domain were  $Dt=0.5\text{ ms}$ ; the numbers of samples was  $M=1000$ . The  
208 near offset (also called origin offset; i.e., the distance between the source point  
209 and the first recording point along the line) of  $x_0=50\text{ cm}$ , the geophone spacing  
210 of  $Dx=50\text{ cm}$  and the offset range of  $L=11.5\text{ m}$  (Figure 3) are the three important  
211 acquisition parameters that require proper selection to prevent aliasing, near  
212 field, and far field effects (Xia et al., 1999 and Miller et al., 1999). These effects  
213 determine the minimum and maximum depth in which Vs can be accurately  
214 measured using the MASW method. Due to certain undesirable effects,  
215 Rayleigh waves must be studied beyond the near field offset. Far from this  
216 distance, they can be considered as horizontally travelling plane waves and  
217 processed accordingly. The adaptation of MASW to soil investigations is first  
218 conditioned by the possibility of reducing the seismic array (originally consisting  
219 of several tens of meters) to approximately several meters, provided that near-  
220 field effects are avoided. Second, the frequency range of the seismic signal is

221 increased to obtain a depth of interest up to a maximum of 10 m below the  
222 ground surface. Finally, the selected seismic system involved a hammer source  
223 that was capable of generating signals in the 1 to few tens of Hz frequency  
224 range; and a seismic antenna composed of 24 geophones capable of recording  
225 signals from 10 to 200 Hz was used. The entire system was towed behind a  
226 vehicle (Figure 3a) to ensure a rapid acquisition. A total of 157 seismic  
227 observations were performed along 13 transects with regular 12 m spaces  
228 between data points, as shown in Figure 1.

229 For step (2), the generation of a dispersion curve is one of the most critical  
230 steps for generating an accurate  $V_s$  profile. Dispersion curves are generally  
231 displayed as  $Cf$  as a function of  $f$  (Figure 5b). For impulsive data, a frequency-  
232 domain approach (Park et al., 1998b) is used to calculate the dispersion curve.  
233 This approach involves a 2D wavefield operation that transforms seismic data  
234 from the space-time domain into the  $Cf$ - $f$  domain, which is more convenient for  
235 highlighting dispersion features.

236 For step (3), the  $V_s$  profiles were calculated using an iterative inversion process  
237 (Tarantola, 1987) that requires dispersion data (Figure 5c). A least-squares  
238 approach allows for the automation of the process (Xia et al., 1999). For the  
239 method used here, only the  $V_s$  and model thickness are updated after each  
240 iteration; Poisson's ratio remains unchanged throughout the inversion. An initial  
241 earth model needed to be specified as a starting point for the iterative inversion  
242 process. The earth model consists of velocity ( $P$ -wave and  $S$ -wave velocity),

243 density, and thickness parameters. Among these four parameters,  $V_s$  has the  
244 most significant effect on the reliable convergence of the algorithm. For each  
245 iteration of the inversion process, an update of  $V_s$  is calculated, and synthetic  
246 dispersion curves are back calculated from this new  $V_s$  model. The synthetic  
247 dispersion curve is then compared to the observed dispersion curve based on  
248 the least-squares method (Figure. 5d). A reliable  $V_s$  model is obtained when the  
249 misfit between synthetic and observed dispersion curves is minimised. The  
250 inversion algorithm used in our study implements all of these aspects and is  
251 based on Hermann (1987). The stop criterion for the  $Cf$  residuals between  
252 synthetic and observed dispersion curves was defined as less than  $5 \text{ m.s}^{-1}$ .  
253 Finally, the interpolation of contiguous  $V_s$  models resulting from the inversion  
254 process is realised using a natural neighbour method to obtain a 2D  $V_s$  section  
255 along the transect.

#### 257 *2. 4. Penetrometer soundings*

258  
259 A dynamic penetrometer with variable energy (Afnor, French norm NF XP P 94-  
260 105) can be used to record the mechanical resistance ( $Qd$  in MPa) variation  
261 with depth (Sanglerat, 1975; Burns and Mayne, 1996) by manually driving a rod  
262 into the soil using a standardised hammer. Therefore, a penetrometer can be  
263 used to identify variations in soil profiles according to the penetration  
264 modulations observed on the rod at each blow of the hammer. Because this

265 method is easy to use and relatively quick, this portable automatic penetrometer  
266 is well adapted for detailed prospecting and mapping (Zhou, 1997). Each  
267 penetrometric sounding (CPT) products a vertical cone resistance profile called  
268 a penetrogram; the interpretation of the penetrogram allows for the identification  
269 of different layers and that estimation of their thickness using two main criteria:  
270 well-defined cone resistance thresholds and the shape of the penetrogram.  $Qd$   
271 is calculated using the following relationship (Langton, 1999):

272

$$273 \quad Qd = \frac{1}{A} \times \frac{\frac{1}{2}MV^2}{e} \times \frac{1}{1 + \frac{P}{M}} \quad (1)$$

274

275 where  $A$  is the cone section ( $2 \text{ cm}^2$ ),  $M$  is the striking mass (kg),  $V$  is the impact  
276 velocity (ratio between the cell spacing and travel time between cells),  $P$  is the  
277 struck mass (kg) and  $e$  is the drill string progress (m).  $Qd$  soundings were  
278 performed using a Dynamic PANDA penetrometer (Gourvès and Barjot, 1995)  
279 along transect n°5 of the field plot with a regular spacing of 12 m; this survey  
280 was conducted at the same location as the collection of seismic data points  
281 (Figure 1). In this study, we assimilated the cone mechanical resistance  $Qd$  into  
282 the soil stiffness.

283

284 *2. 5. Drilling observations*

285

286 In addition to the abovementioned surveys, 4 drilling observations were  
287 performed on the same transect with a spacing of 40 m in the midslope and 20  
288 m in the footslope regions (Figure 1). Each borehole was excavated in the  
289 north-west to south-east direction to depths of 1.85 m, 3.5 m, 6 m and 1.7 m.  
290 Drilling cores were used to estimate *ThickLM* and for laboratory measurements  
291 of the water content ( $\theta$ ), the real density of the solid ( $\rho_r$ ) and the bulk density  
292 (i.e., the density of the sample as a whole) ( $\rho_b$ ) in the loamy layer; these results  
293 are shown in Table 1.

294

## 295 2. 6. Sensitivity of Vs to soil mechanical properties

296

297 Numerical relationships between soil mechanical properties and Vs have  
298 been previously published. One of these relationships, which is given by elastic  
299 theory and is an essential property for evaluating dynamic responses and the  
300 stiffness of soil, is the small-strain shear modulus, G (i.e., a measure of solidity).  
301 Values of G are typically determined indirectly by measuring the shear wave  
302 velocity, Vs, and the mass density of the soil,  $\rho$ , and computing  $G = \rho V_s^2$ . Other  
303 commonly used relationships include the correlation between cone penetration  
304 resistance or SPT blow count (N) and Vs and functional forms; this relationship  
305 is reported to be  $V_s = A.N^B$ , where the constants A and B are determined by a  
306 statistical regression of a data set. A significant number of correlations have

307 been published for various soil types. Imai and Yoshimura (1975) studied the  
308 relationship between seismic velocities and certain index properties for 192  
309 samples and developed empirical relationships for all soil types. Sykora and  
310 Stokoe (1983) reported that geological age and type of soil are not predictive of  
311  $V_s$ , whereas the uncorrected SPT-N value is the most important term. Sykora  
312 and Koester (1988) demonstrated a strong statistical correlation between the  
313 dynamic shear resistance and standard penetration resistance of soils. Iyisan  
314 (1996) examined the influence of the soil type on the correlation between SPT-  
315 N and  $V_s$  using data collected from an earthquake-prone area in the eastern  
316 part of Turkey. The results showed that with the exception of gravels, the  
317 correlation equations developed for all soils, sand and clay yield approximately  
318 similar  $V_s$  values. Jafari et al. (2002) presented a detailed historical review of  
319 the statistical correlation between SPT-N and  $V_s$ . Hasancebi and Ulusay (2006)  
320 studied similar statistical correlations using 97 data pairs collected from an area  
321 in the north-western part of Turkey and developed empirical relationships for  
322 sands, clays, and all soils irrespective of soil type. Ulugergerli and Uyanik  
323 (2007) investigated statistical correlations using 327 samples collected from  
324 different areas of Turkey and defined the upper and lower bounds of an  
325 empirical relationship instead of a single average curve for estimating seismic  
326 velocities and relative densities.

327 These previous studies, as well as a qualitative comparison of data available on  
328 our study site, demonstrate the good correlation of  $V_s$  to soil mechanical

329 properties and allow for the expectation of a relatively good characterisation of  
330 StiffLM using Vs and an accurate estimation of ThickLM (Figure 6) in this  
331 context.

332

### 333 **3. Evaluation of ThickLM and StiffLM of the loamy material horizon**

334

#### 335 *3. 1. Relationships between Vs and CPTs*

336 The distribution of Vs values inverted along the transect n°5 allowed for the  
337 discrimination between two populations that corresponded to different  
338 mechanical properties. Each population was characterised by Gaussian laws of  
339  $\text{mean}_{1\text{st layer}} = 171 \text{ m.s}^{-1}$ ,  $\sigma_{1\text{st layer}} = 80 \text{ m.s}^{-1}$  and of  $\text{mean}_{2\text{nd layer}} = 347 \text{ m.s}^{-1}$ ,  $\sigma_{2\text{nd}}$   
340  $\text{layer} = 76 \text{ m.s}^{-1}$ , where  $\sigma$  is the standard deviation (Figure 7). Moreover, the  
341 isovalue of  $V_s=240 \text{ m.s}^{-1}$  was highly consistent with the isovalue  $Q_d=20 \text{ MPa}$ ,  
342 which marks the boundary between a soft superficial unit and a competent  
343 underlying formation (Figure 8). This observation was then used for the  
344 calibration of a Vs threshold value ( $V_{s\text{Lim}} = 240 \text{ m.s}^{-1}$ ) to characterise a  
345 mechanical limit used as a criteria to map ThickLM over the entire field based  
346 on the entire seismic dataset. Finally, the mean squared error (MSE) between  
347 ThickLM observations and estimations were computed using a validation set of  
348 4 drilling points that were positioned to be representative of the observed main  
349 variability of ThickLM.

350 To study the stiffness of the loamy material-horizon, we compared  $V_s$  and  $Q_d$ ,  
 351 obtained by CPTs, at a same depth. The two parameters can be interrelated  
 352 because they are both influenced by effective level of confining stress, the  
 353 anisotropic  $K_0$ -stress state, mineralogy, aging, bonding, and other factors  
 354 (Mayne and Rix, 1995; Stuedlein, 2010; Dikmen, 2009). We first applied an  
 355 exclusion filter to the  $V_s$  data with the condition  $V_s < V_{sLim}$  to restrict the  
 356 analysis to the loamy layer. Then, we computed the average  $Q_d$  values in each  
 357 interval of  $V_s$  1D models. Nugget effects on the  $Q_d$  data, which occur due to the  
 358 punctual presence of various defects (e.g., pebbles) in the medium, were  
 359 previously removed from the dataset using an interpolating operator. Figure 9  
 360 shows the linear regression between  $V_s$  and  $Q_d$  where a correlation between  
 361  $Q_d$  and  $e^{V_s}$  is observed with  $R^2=0.4$  and a two-tailed  $P$  value less than 0.0001.  
 362 By conventional criteria, this difference is considered to be extremely  
 363 statistically significant even if samples are highly scattered. Therefore, we  
 364 predicted  $Q_d$  according to  $V_s$  using the following equation:

365

$$366 \quad Q_d = 1.2965e^{0.0057V_s} \quad R^2 = 0.4 \quad P < 0.0001 \quad (2)$$

367

368 Mapping of the spatial variation of *StiffLM* as a function of the average  $Q_d$   
 369 calculated over *ThickLM* using Eq. (2) then becomes possible over the entire  
 370 field. Density comparisons between the  $\rho_b$  measured for the drill samples and  
 371 the  $\rho_b$  calculated from  $V_s$  using published relationships (Mayne, 2001) were

372 also performed, and no significant correlations were determined. This absence  
373 of correlations was probably due to the lack of  $\rho_b$  values for the clay formation.

374

### 375 3. 2. Spatial structure and interpolation of the data

376

377 The spatial structures of *ThickLM* and *StiffLM* were assessed using variograms  
378 that were estimated in four directions at 20°, 55°, 110° and 155° from  
379 geographic north. The variograms were generated using all possible sample  
380 pairs in a given direction and by grouping these into classes (lags) of  
381 approximately equal distance (Matheron, 1965). The variances (one-half of the  
382 mean squared difference) of these paired sample measurements were then  
383 plotted as a function of the distance between samples to provide a means of  
384 quantifying the spatial structure of the data. *ThickLM* and *StiffLM* obtained using  
385 *MASW* and Eq. (2), respectively, were then interpolated using ordinary kriging.  
386 Ordinary kriging is a geo-statistical method that takes into account both the  
387 distance and the degree of variation between known data points and relies on  
388 the spatial correlation structure of the data to determine the weighting values.  
389 This type of kriging has been shown to provide better performance for soil  
390 parameters than other available methods (e.g., Burgess et al., 1981; Myers,  
391 1994). The interpolations were accomplished by fitting each of several  
392 theoretical variogram models (i.e., linear, Gaussian, spherical, and exponential  
393 models) to the empirical isotropic variogram using the least-squares method.

394 The best fit model was then used for the interpolation. Data points were  
395 subsequently interpolated to a regular 2×2 m grid using a full second-order  
396 polynomial drift function, which is the common practice.

397

#### 398 **4. Results**

399

400 *ThickLM* ranged between 0.2 and 6.5 m with an average of 2.6 m and a median  
401 of 2.7 m (Table 2; Figure 10a). As shown by the variogram analysis (Figure  
402 11a), *ThickLM* exhibited a moderate anisotropy and spatial structure.  
403 Nevertheless, a slight azimuth dependence of less and greater variability was  
404 observed at the the 20° and 110° directions, respectively, relative to the other  
405 directions of less and greater variability than the other directions. The  
406 observations were interpolated over the 120×130 m plot and using an  
407 exponential model (sill = 0.75; range = 4.5 m) coupled with a Gaussian model  
408 (sill = 9; range = 70 m). The interpolated *ThickLM* map showed a gradual  
409 increase in thickness from the north-west limit of the plot, where values were  
410 approximately 0.20 m, to the mid-plot position; a gradual decrease was then  
411 observed from the mid-plot position to the south-east limit, where *ThickLM* was  
412 approximately the same as on the north-west side (Figure 10a). An area of  
413 greater *ThickLM* (between 3 and 6.5 m) was observed at the mid-plot position.  
414 A local area of greater *ThickLM* (between 1.5 and 3 m) was observed on the  
415 north-west side of the plot. The differences between the observed and

416 estimated ThickLM values are shown in Figure 12. The MSE of 0.043 m and  
417  $R^2=0.956$  between these two variables over the 4 validation points shows that  
418 the estimated ThickLM could be considered to be accurate based on the  
419 consideration that the drilling observations are determined to be representative  
420 of the overall observed variability of ThickLM over the entire plot.

421 *StiffLM*, which is related to the mean *Qd* calculated over *ThickLM*, ranged  
422 between 2 and 6 MPa with an average of 3.78 MPa and a median of 3.68 MPa  
423 (Table 2; Figure 10b). As demonstrated by the variogram analysis (Figure 11b),  
424 *StiffLM* exhibited a moderate anisotropy and spatial structure. Anisotropy was  
425 observed between the 20 and 110° directions with less and greater variability  
426 than the other directions. The observations were interpolated over the 120×130  
427 m plot using a Gaussian model (nugget = 0.1; sill = 0.7; range = 50 m). The  
428 interpolated *StiffLM* map showed a gradual decrease in stiffness from the north-  
429 west limit of the plot, where the values range between 5 and 6 MPa, to the mid-  
430 plot position; a gradual increase from mid-plot position to the south-east limit,  
431 where *StiffLM* presented a lower stiffness than on the north-west side, was  
432 also observed (Figure 10b). An area of lower *StiffLM* (between 2 and 4 MPa)  
433 was observed at the mid-plot position. A local zone of lower *StiffLM*  
434 (approximately 4 MPa) was observed in the north-west side of the plot.

435

## 436 5. Discussion

437

438 The maps of *ThickLM* and *StiffLM* were in good agreement with the expected  
439 consequences of the on-going erosion of the loamy material horizon: a  
440 gradation in the thickness of the loamy material-horizon from thick and well  
441 conserved in the lower parts to thin and eroded in the upper parts, was  
442 observed (Figure 10a). The increase of *StiffLM* at the limits of the study plot  
443 shows clear evidence of soil degradation in the north-western and south-  
444 eastern zones with the presence of bare soils and outcropping clays and flints,  
445 which have a mechanical resistance. The local event of greater *ThickLM* and  
446 lower *StiffLM* indicated on Figures 10a and 10b with a black dotted line should  
447 correspond to a buried former gully that was photographed at this location 2  
448 years prior to the study and was caused by strong runoff activity (Figure 10c).  
449 This structural and mechanical characterisation of the loamy material horizon  
450 should not only help to focus conservation measures in the most threatened  
451 areas (i.e., areas that show a reduced *ThickLM* and increased *StiffLM*  
452 associated with high soil erosion vulnerability and/or a high compaction state),  
453 but will also help identify historical erosion events. The combination of maps of  
454 soil stiffness and surficial sediment depths will allow the development and  
455 implementation of soil conservation measures to target high-priority areas.  
456 Where climatic scenarios are available, these maps can also be used to  
457 calculate the potential productivity loss using simulators, such as the  
458 SimPLE.ca model (Bremer et al., 2008). This method will also contribute to the  
459 broad discussion of reducing the inherent uncertainty in current soil mapping or

460 attribute determinations. Soil maps show that there can be considerable  
461 uncertainty in map unit composition with resulting spatial variability in soil  
462 properties within map units (Webb and Lillburne, 2005). Actual soil maps define  
463 discrete soil classes, which represent the interpolation of only a limited number  
464 of modal soil profiles without capturing the full extent of soil variability (Campbell  
465 and Edmonds, 1984; Qi and Zhu, 2011). In the study presented here, the non-  
466 destructive mapping of continuous soil properties in space will help to improve  
467 the data frequency and allow for the derivation of probability distributions to  
468 parameterise the fuzzy nature of the geographical objects that comprise the soil  
469 maps (Martin-Clouaire et al., 2000).

470  
471

472

## 473 **6. Conclusions**

474

475 The objective of this study was to test and validate a new geophysical technique  
476 for mapping soil properties that are related to soil erosion processes. A seismic  
477 experiment coupled with penetrometric measurements form the basis of the  
478 proposed methodology. The MASW method was efficient for producing Vs  
479 models over large areas. When coupled with penetrometric measurements of  
480 Qd variations with depth, high-resolution maps of soil thickness and stiffness

481 can be produced, provided that a correlation is found to occur between Vs and  
482 Qd.

483 We demonstrated that accurate mapping of variations in the thickness and  
484 stiffness of the loamy material horizon can be obtained by integrating  
485 information on the relationship between seismic Vs, soil mechanical resistance  
486 and drilling observations into the mapping process. An analysis of the  
487 correlation between seismic Vs and soil mechanical behaviours provided an  
488 effective basis for the accurate delineation of a specific soil attribute. According  
489 to the discussion, the analysis of the correlation between the seismic shear  
490 wave velocity and the soil bulk density at an interface of strongly contrasted  
491 mechanical properties should be studied further.

492 The future of precise mapping of selected soil properties using geophysical  
493 seismic techniques is dependent on the understanding of relationships between  
494 geophysical signals obtained from this technology and the overall spatial and  
495 temporal variability of soil patterns. As the value of the soil resources and  
496 associated ecological services receive greater recognition, digital soil mapping  
497 based on seismic shear wave velocity can provide spatial data regarding soil  
498 degradation that will serve as an essential tool for soil conservation and/or soil  
499 rehabilitation.

500

## 501 **5. Acknowledgements**

502

503 This study was funded by the FP7-DIGISOIL project. The DIGISOIL project  
504 (FP7-ENV-2007-1 N°211523) is financed by the European Commission under  
505 the 7th Framework Programme for Research and Technological Development,  
506 Area “Environment”, Activity 6.3 “Environmental Technologies”. The authors  
507 thank J. F. Ouvry from AREAS for his help in focusing the study field and Alexis  
508 Rochat for his help in acquiring field seismic data. Finally, the authors thank the  
509 editors of *Geoderma* and two anonymous reviewers for their comments and  
510 suggestions that led to an improved version of the manuscript.

511

## 512 6. References

513

514 Afnor, Norme française NF XP P 94-105, Essai de pénétration dynamique à  
515 énergie variable, Association française de normalisation, 2000.

516 Azaria, A., C. Zelt, A. Levander, 2003. High-resolution seismic mapping at a  
517 groundwater contamination site: 3-D travelttime tomography of refraction  
518 data, EGS-AGU-EUG Joint Meeting, Nice, France.

519 Biot Y, Lu X.X. 1995. Loss of yield caused by soil erosion on sandy soils in the  
520 UK, *Soil use and Management* 11 (4)157-162.

521 [Bremer E., Black M., Townley-Smith L., Malhi SS., Izaurralde RC., Larney FJ.](#)  
522 [2008. SimPLE.ca: Simulator of productivity loss due to erosion for](#)  
523 [Canada, \*Canadian Journal of Soil Sciences\* 88 \(3\) 365-376.](#)

- 524 Bullen, K. E., 1963, An introduction to the theory of seismology: Cambridge  
525 Univ. Press.
- 526 Burgess, T., Webster, R., McBratney, A., 1981. Optimal interpolation and  
527 isarithmic mapping of soil properties. IV. Sampling strategy. J. Soil Sci. 32,  
528 643–659.
- 529 Burns, S.E., Mayne, P.W., 1996. Small and high-strain measurements of in-situ  
530 soil properties using the seismic cone penetrometers. TRR 1548 Small-  
531 Magnitude Measurements in Geotechnical Engineering. National Academy  
532 Press, pp. 81-88.
- 533 J.B. Campbell and W.J. Edmonds, 1984. The missing geographic dimension to  
534 soil taxonomy. Annals of the Association of American  
535 Geographers, 74 (1984), pp. 83–97.
- 536 Cerdan O., G. Govers, Y. Le Bissonnais, K. Van Oost, J. Poesen, N. Saby, A.  
537 Gobin, A. Vacca, J. Quinton, K. Auerswald, A. Klik, F.J.P.M. Kwaad, D.  
538 Raclot, I. Ionita, J. Rejman, S. Rousseva, T. Muxart, M.J. Roxo, T. Dostal.  
539 2010. The rate and spatial distribution of soil erosion in Europe,  
540 Geomorphology 122, 167-177.
- 541 Chaplot, V., Walter, C., Curmi, P., Hollier-Larousse, A., 2001. Mapping field-  
542 scale hydromorphic horizons using Radio-MT electrical resistivity.  
543 Geoderma 102, 61–74.

- 544 Debeglia N., Bitri A., Thierry P., 2006. Karst investigations using microgravity  
545 and MASW; Application to Orléans, France. *Near Surface Geophysics*, 4,  
546 215-225.
- 547 Dikmen, U., 2009. Statistical correlations of shear wave velocity and penetration  
548 resistance for soils. *Journal of Geophysics and Engineering*, volume 6,  
549 number 1.
- 550 Eigenberg, R.A., Korthals, R.L., Neinaber, J.A., 1998. Geophysical  
551 electromagnetic survey methods applied to agricultural waste sites. *J.*  
552 *Environ. Qual.* 27, 215–219.
- 553 European Commission (2002). *Towards a strategy for soil protection*, COM  
554 (2002) 179 final. Internet:[http://europa.eu.int/comm/environment/  
555 agriculture/soil\\_protection.htm](http://europa.eu.int/comm/environment/agriculture/soil_protection.htm).
- 556 European Commission. 2006. Thematic Strategy for Soil Protection,  
557 COM(2006)231 final. Internet: [http://eur-lex.europa.eu/LexUriServ/Lex  
558 UriServ.do?uri=COM:2006:0231:FIN:EN:PDF](http://eur-lex.europa.eu/LexUriServ/LexUriServ.do?uri=COM:2006:0231:FIN:EN:PDF)
- 559 Foti, S., (2000) Multistation Methods for Geotechnical Characterization using  
560 Surface-waves, Dottorato di Ricerca in Ingegneria Geotecnica.
- 561 Gourvès, R., Barjot, R., 1995. Le pénétromètre dynamique léger Panda.  
562 Comptes rendus, 11ème congrès Européen de Mécanique des Sols et  
563 des Travaux de Fondations, Copenhague, vol. 3, 83-88.

- 564 Grandjean G. and Bitri A., (2006) 2M-SASW: inversion of local Rayleigh wave  
565 dispersion in laterally heterogeneous subsurfaces: application to Super-  
566 Sauze landslide (France). *Near Surface Geophysics*,, 367-375.
- 567 Grandjean, G., 2006a. A seismic multi-approach method for characterizing  
568 contaminated sites. *J. Applied Geophys.*, 58, 87-98.
- 569 Grandjean G., 2006b. Imaging subsurface objects by seismic P-wave  
570 tomography: numerical and experimental validations. *Near Surface*  
571 *Geophysics*, 275-283.
- 572 Grandjean, G., Malet, J.P., Bitri, A., and Meric O., 2007. Geophysical data  
573 fusion by fuzzy logic for imaging mechanical behaviour of mudslides. *Bull.*  
574 *Soc. Geol. France*, 177, 2, 133-143.
- 575 Hadgu KM., Rossing WAH., Kooistra L., van Bruggen AHC. 2009. Spatial  
576 variation in biodiversity, soil degradation and productivity in agricultural  
577 landscapes in the highlands of Tigray, northern Ethiopia, *Food Security* 1  
578 (1) 83-97.
- 579 Hasancebi, N. and Ulusay, R. (2006). "Empirical correlations between shear  
580 wave velocity and penetration resistance for ground shaking assessments,"  
581 *Bull Eng Geol Environ*, 66, 203-213.
- 582 Heckrath G, Djurhuus J, Quine TA, Van Oost K, Govers G, Zhang Y. 2005.  
583 Tillage erosion and its effect on soil properties and crop yield in Denmark,  
584 *Journal of Environmental Quality* 34 (1) 312-324.

- 585 Hermann, R.B., 1987. Computer programs in seismology. Saint-Luis University,  
586 USA.
- 587 Imai, T. and Yoshimura, Y. (1975). "The relation of mechanical properties of  
588 soils to P and S-wave velocities for ground in Japan," *Technical Note*, OYO  
589 Corporation. Iyisan, R. (1996). "Correlations between shear wave velocity  
590 and in-situ penetration test results," *Tech. J. Chamber Civil Eng. Turkey*, 7,  
591 1187–99 (in Turkish).
- 592 Jafari, M. K., Shafiee, A. and Ramzkhah, A. (2002). "Dynamic properties of the  
593 fine grained soils in south of Tehran," *J. Seismol. Earthq. Eng.*, 4, 25–35.
- 594 Kachanoski, R.G., Gregorich, E.G., Van Wesenbeeck, J., 1988. Estimating  
595 spatial variations of soil water content using noncontacting  
596 electromagnetic inductive methods. *Can. J. Soil Sci.* 68, 715–722.
- 597 Kalinski, R.J., Kelly, W.E., 1993. Estimating water content of soils from electrical  
598 resistivity. *Geotech. Test. J.* 16, 323–329.
- 599 Langton, D. D., 1999. The PANDA lightweight penetrometer for soil  
600 investigation and monitoring material compaction, Ground Engineering.
- 601 Lanz, E., Mauer, H., Green, A.G., 1998. Refraction tomography over a buried  
602 waste disposal site. *Geophysics* 63, 1414– 2007-02-21.
- 603 Lunne, P., Robertson, P. KK., and Powell, J. J. M., 1997, Cone penetration  
604 testing in geotechnical practice. E and FN SPON.

- 605 [Martin-Clouaire R., Cazemier D.R., Lagacherie P. 2000. Representing and](#)  
606 [processing uncertain soil information for mapping soil hydrological](#)  
607 [properties Computers and Electronics in Agriculture 29 \(1-2\), 41-57](#)
- 608 Matheron, G., 1965. Les variables régionalisées et leur estimation: une  
609 application de la théorie de fonctions aléatoires aux sciences de la nature.  
610 Masson et Cie, Paris. 306 pp.
- 611 Mayne, P.W., 2001, Stress-strain-strength-flow parameters from enhanced in-  
612 situ tests, *Proceedings of the International Conference on In-Situ*  
613 *Measurement of Soil Properties and Case Histories, Bali, pp. 27-48.*
- 614 Mayne, P. W., Rix, G. J., Correlations between shear wave velocity and cone tip  
615 resistance in natural clays, *Soil and Foundations* 35 (1995) (2), pp. 107–  
616 110.
- 617 McMechan G. A., Yedlin M. J., 1981, Analysis of dispersive waves by wave field  
618 transformation. *Geophysics* vol. 46 p. 869-874.
- 619 Michot, D., Benderitter, Y., Dorigny, A., Nicoullaud, B., King, D., Tabbagh, A.,  
620 2003. Spatial and temporal monitoring of soil water content with an  
621 irrigated corn crop cover using electrical resistivity tomography. *Water*  
622 *Resour. Res.* 39, 11–38.
- 623 Miller, R.D., Xia, J., Park, C.B., and Ivanov, J.M., 1999, Multichannel analysis of  
624 surface waves to map bedrock: *The Leading Edge*, 18, 1392–1396.
- 625 Myers, D.E., 1994. Spatial interpolation: an overview. *Geoderma* 62, 17–28.

- 626 Nazarian, S., Stokoe, K. H., II, and Hudson, W. R., 1983, Use of spectral analysis  
627 of surface waves method for determination of moduli and thicknesses of  
628 pavement systems: *Transport. Res. Record*, **930**, 38–45.
- 629 Papy F, Douyer C. 1991. Influence des états de surface du territoire agricole sur  
630 le déclenchement des inondations catastrophiques. *Agronomie* **11**: 201–215.
- 631 Park, C.B., Miller, R.D., Xia, J., Ivanov, J., 2000. Multichannel seismic surface-  
632 wave methods for geotechnical applications. Proc. of the First Int. Conf. on  
633 the App. of Geophys. Methodologies to Transportation Facilities and  
634 Infrastructure, St. Louis, December 11–15.
- 635 Park, C.B., Miller, R.D., and Xia, J., 1999a, Multimodal analysis of high  
636 frequency surface waves: *Proceedings of the symposium on the*  
637 *application of geophysics to engineering and environmental problems '99*,  
638 115–121.
- 639 Park, C.B., Miller, R.D., and Xia, J., 1999b, Multichannel analysis of surface  
640 waves: *Geophysics*, **64**, 800–808.
- 641 Park, C. B., Xia, J., and Miller, R. D., 1998a, Ground roll as a tool to image  
642 near-surface anomaly: 68th Ann. Internat. Mtg., Soc. Expl. Geophys., Expanded  
643 Abstracts, 874–877.
- 644 Park, C. B., Xia, J., and Miller, R. D., 1998b, Imaging dispersion curves of  
645 surface waves on multichannel record: 68th Ann. Internat. Mtg., Soc. Expl.  
646 Geophys., Expanded Abstracts, 1377–1380.

- 647 [Qi F., Zhu A-X. 2011. Comparing three methods for modeling the uncertainty in](#)  
648 [knowledge discovery from area-class soil maps Computers &](#)  
649 [Geosciences 37 \(9\), 1425-1436](#)
- 650 Rejman J., I. Iglík. 2010. Topsoil reduction and cereal Yields on loess soils of  
651 Southeast Poland Land Degrad. Develop. 21: 401–405.
- 652 Richart, F. E., Hall, J. R., and Woods, R. D., 1970, Vibrations of soils and  
653 foundations: Prentice-Hall, Inc.
- 654 Rhoades, J.D., Corwin, D.L., 1981. Determining soil electrical conductivity-  
655 depth relations using inductive electromagnetic soil conductivity meter.  
656 Soil Sci. Soc. Am. J. 45, 255–260.
- 657 Rhoades, J.D., van Schilfgaarde, J., 1976. An electrical conductivity probe for  
658 determining soil salinity. Soil Sci. Soc. Am. J. 40, 647–651.
- 659 Robain, H., Descloitres, M., Ritz, M., Atangana, Q.Y., 1996. A multiscale  
660 electrical survey of a lateritic soil system in the rain forest of Cameroon. J.  
661 Appl. Geophys. 34, 237–253.
- 662 Samouëlian, A., Cousin, I., Tabbagh, A., Bruand, A., Richard, G., 2005.  
663 Electrical resistivity survey in soil science: a review. Soil Tillage Res. 83,  
664 173–193.
- 665 Sanglerat. G, The penetrometer and soil exploration, Elsevier, 1975.
- 666 Stokoe, K. H., II, Wright, G. W., James, A. B., and Jose, M. R., 1994,  
667 Characterization of geotechnical sites by SASW method, *in*Woods, R. D., Ed.,  
668 Geophysical characterization of sites: Oxford Publ.

669 Stuedlein, A. W., 2010. Shear-wave velocity correlations for Puyallup River  
670 alluvium, *J. Geotech. and Geoenviron. Engrg.* 136, 1298 (2010 );  
671 doi:10.1061/(ASCE)GT.1943-5606.0000342 (7 pages)

672 Sturtevant, K. A., Baker, G. S., Snyder, C., Kopczynski, S., 2004.  
673 Hydrogeophysical characterization of bedrock fracture orientations using  
674 azimuthal seismic refraction tomography. AGU, H23A-1122.

675 Sykora, D. E. and Stokoe, K. H. (1983). "Correlations of in-situ measurements  
676 in sands of shear wave velocity," *Soil Dyn. Earthq. Eng.*, 20, 125–36.

677 Sykora, D. W. and Koester, P. J. (1988). "Correlations between dynamic shear  
678 resistance and standard penetration resistance in soils," *Earthq. Eng. Soil  
679 Dyn.*, 2, 389–404.

680 Tarantola, A., 1987, *Inverse problem theory*. Elsevier Science Publishing Co.,  
681 Inc.

682 Tengberg A, Stocking M, Dechen SCF. 1997. The impact of erosion on soil  
683 productivity - An experimental design applied in Sao Paulo State, Brazil,  
684 *Geografiska Annaler Series A, Physical Geography* 79A (1-2) 95-107.

685 Thompson, J.A., Bell, J.C., 1996. Color index for identifying hydric conditions for  
686 seasonally saturated mollisols in Minnesota. *Soil Sci. Soc. Am. J.* 60,  
687 1979–1988.

688 Ulugergerli, U. E. and Uyanik, O. (2007). "Statistical correlations between  
689 seismic wave velocities and SPT blow counts and the relative density of  
690 soils," *J. Test. Eval.*, 35, 1–5.

- 691 U.S. Department of Agriculture, 2003. National Soil Survey Handbook, title 430-  
692 VI. [Online] Available: [http:// soils.usda.gov/technical/handbook/N](http://soils.usda.gov/technical/handbook/N).
- 693 Van-Camp. L., Bujarrabal, B., Gentile, A-R., Jones, R.J.A., Montanarella, L.,  
694 Olazabal, C. and Selvaradjou, S-K. (2004). Reports of the Technical  
695 Working Groups Established under the Thematic Strategy for Soil  
696 Protection. EUR 21319 EN/1, 872 pp. Office for Official Publications of the  
697 European Communities, Luxembourg.
- 698 [Webb, TH, Lilburne, LR. 2005 Consequences of soil map unit uncertainty on](#)  
699 [environmental risk assessment AUSTRALIAN JOURNAL OF SOIL](#)  
700 [RESEARCH 43 \(2\), 119-126](#)
- 701 Williams, B.G., Hoey, D., 1987. The use of electromagnetic induction to detect  
702 the spatial variability in the salt and clay content of soils. *Austr. J. Soil Res.*  
703 25, 21–27.
- 704 World Reference Base, 1998. World Reference Base for Soil Resources. FAO,  
705 World Resources Report no. 84, Rome, Italy.
- 706 Xia, J., Miller, R.D., and Park, C.B., 1999, Configuration of near surface shear  
707 wave velocity by inverting surface wave: *Proceedings of the symposium*  
708 *on the application of geophysics to engineering and environmental*  
709 *problems '99*, 95–104.
- 710 Ye L., Van Ranst E. 2009. Production scenarios and the effect of soil  
711 degradation on long-term food security in China, *Global Environmental*  
712 *Change* 19 464–481.

713 Zhou. S, Caractérisation des sols de surface à l'aide du pénétromètre  
714 dynamique léger à énergie variable type Panda, thèse, université Blaise-  
715 Pascal, Clermont-Ferrand-2, 1997, 179 p.

716

717 **7. Tables**

718

719 Table 1. Soil properties for 4 drilling observations along the n°5 transect with a  
720 spacing of 40 m in the middleslope and 20 m in the downslope (Figure 1).  $\theta$ :  
721 water content,  $\rho_r$ : real density,  $\rho_b$ : bulk density, ThickLM: thickness of the loamy  
722 material horizon, Depth: sample depth, Depth Bis: replicate sample depth.

723

724 Table. 2. General statistics (Min: minimum; Max: maximum; Av: average;  
725 Median; Stdev, standard deviation; Var: variance; CV, coefficient of variation;  
726 Skwe, skewness; Kurt, kurtosis for *ThickLM*, which is the thickness of the loamy  
727 material horizon (m);  $Q_d$ : the mechanical resistance (MPa).

728

729 **8. Figure captions**

730

731 Figure 1. Location of the study plot within the Bourville catchment in Normandy,  
732 a region of Northern France. Contour lines of absolute altitude with 0.5 m  
733 intervals within the 120×130 m plot are presented for the 157 data points of the  
734 seismic survey. Position of the 4 drilling events and the 12 penetrometer  
735 soundings are indicated along the n°5 transect.

736

737 Figure 2. Loamy sediments showing the critical thickness are rendered more  
738 vulnerable to runoff and water erosion relative to competent and nearly  
739 outcropping clays enriched with flints.

740

741 Figure 3. a) Photograph of the towing system with the seismic acquisition  
742 central and laptop computer. b) Photograph of the seismic array with 24  
743 geophones regularly spaced at 50 cm. c) Schematic representation of the  
744 acquisition configuration with the key parameters: near offset  $x_0$ , geophone  
745 spacing  $Dx$  and offset range  $L$ .

746

747 Figure. 4. Workflow diagram illustrating the methodology using to obtained  
748 reliable Vs versus depth models.

749

750 Figure 5. a) Example of recorded surface waves. b) Observed dispersion curve  
751 obtained by  $Cf-f$  domain transformation. c) Comparison between the initial and  
752 final  $V_s$  versus depth model obtained after the inversion step. d) Comparison  
753 between observed and synthetic dispersion curves. The relatively good fit  
754 between these curves indicates the reliability of the final model.

755 Figure 6. Qualitative comparison between a drilling observation, a penetrometer  
756 sounding and a  $V_s$  versus depth model at the same location. The relatively  
757 good correlations between  $V_s$ , mechanical properties of the soil and the  
758 observed lithologies are shown.

759

760 Figure 7. Representation of the  $V_s$  distribution. Two populations characterised  
761 by Gaussian laws of mean<sub>1st layer</sub> = 171 m.s<sup>-1</sup>,  $\sigma_{1st layer}$  = 80 m.s<sup>-1</sup> and of mean<sub>2nd</sub>  
762 layer = 347 m.s<sup>-1</sup>,  $\sigma_{2nd layer}$  = 76 m.s<sup>-1</sup> are distinguished.

763

764 Figure 8. Seismic and penetrometric sections along transect n°5. Threshold  
765 values of  $V_s=240$  m/s and  $Q_d=20$  MPa overlay the sections in black dotted line  
766 and red solid line, respectively. Drilling observations overlay the seismic section  
767 in black crosses. There is a good agreement, in terms of *ThickLM*, between the  
768 threshold values and *ThickLM* obtained from drilling observations.

769

770 Figure. 9. Observed  $V_s$  after exclusion filtering ( $V_s > 240$  m/s) versus averaged  
771 interpolated  $Qd$  computed for the thicknesses of  $V_s$  intervals on 1D models  
772 along the n°5 transect.

773

774 Figure 10. a) Spatial variations in the thickness of the loamy material horizon  
775 (*ThickLM*) obtained using *MASW*. b) Spatial variations in the stiffness of the  
776 loamy material horizon (*StiffLM*) obtained using Eq. (2). Contour lines of  
777 absolute altitude with a 0.5 m interval overlay the map. The 4 drilling  
778 observations, 12 penetrometric data points and 157 seismic data points are  
779 shown on the map. The black dotted line represents the buried former gully that  
780 is visible in the photograph. c) Photograph showing the buried former gully.

781

782 Figure 11. a) Directional variogram of *ThickLM*. b) Directional variogram of  
783 *StiffLM*.

784

785 Figure 12. Plot of estimated *ThickLM* values obtained using the *MASW*  
786 methodology and the observed *ThickLM* for the 4 drilling observations.

787

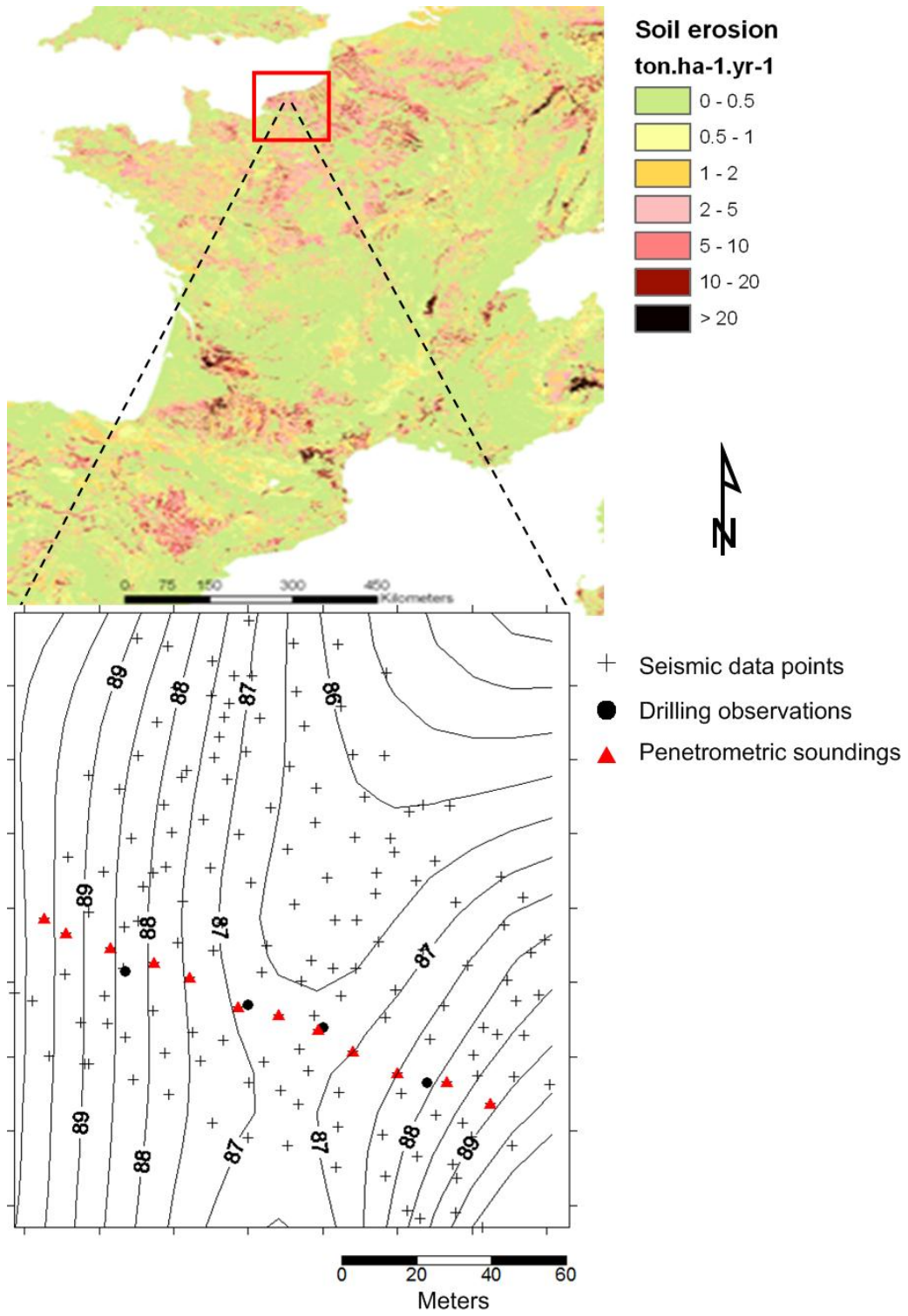
788

789

790

791

792 Figure 1



793

794 Figure 2

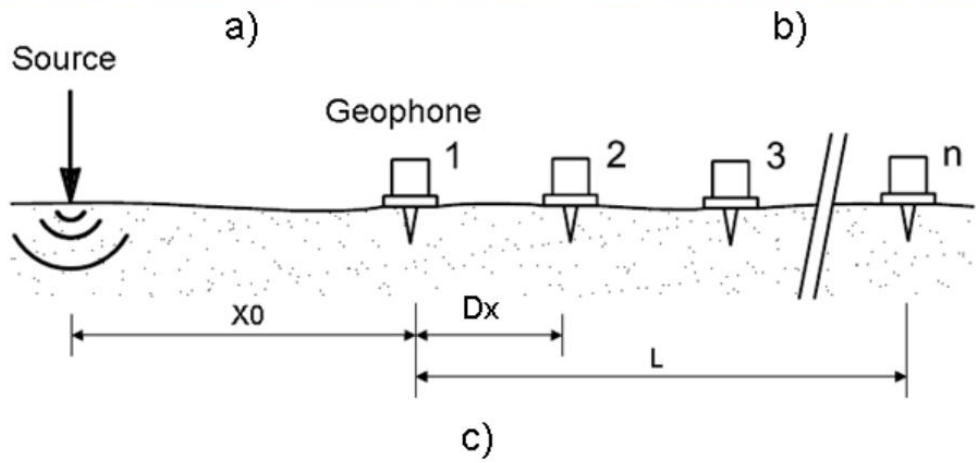
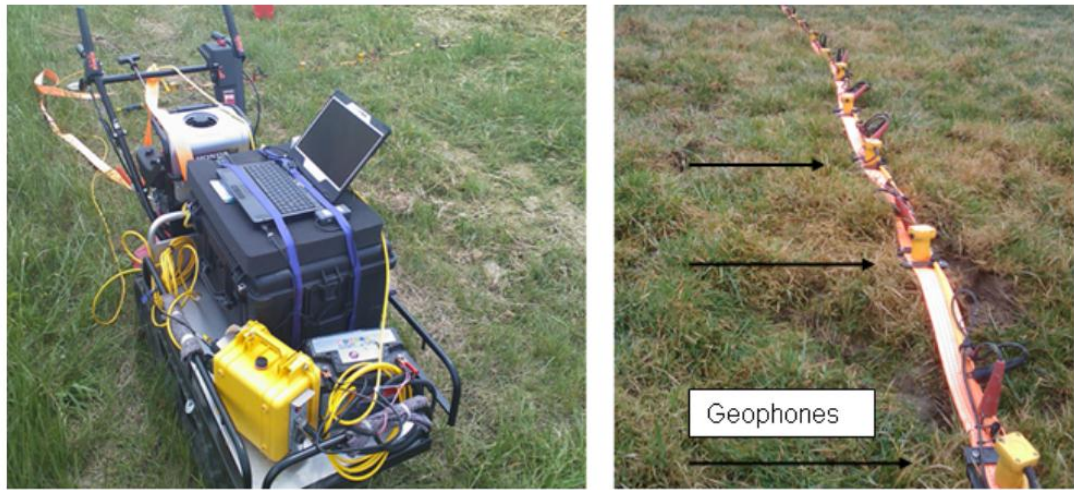


795

796

hal-00658933, version 1 - 11 Jan 2012

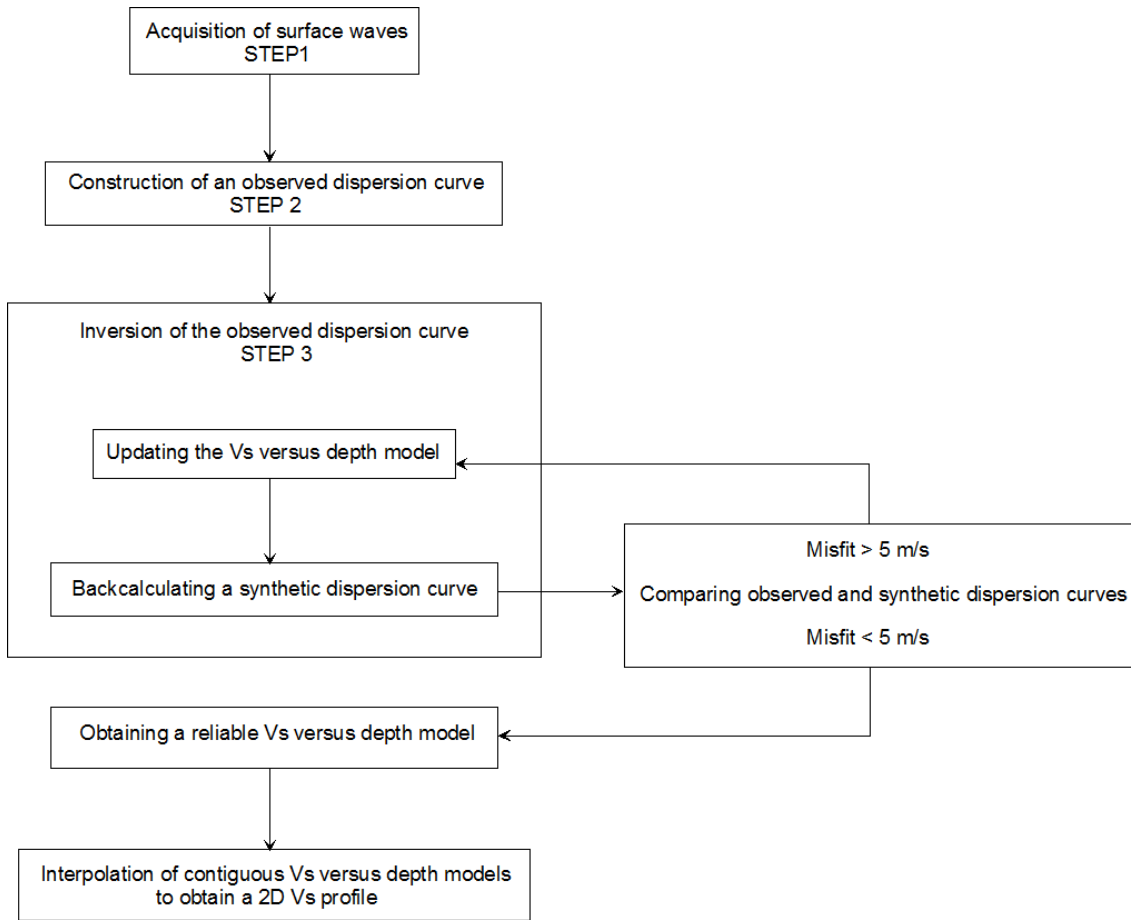
797 Figure 3



798

799

800 Figure 4

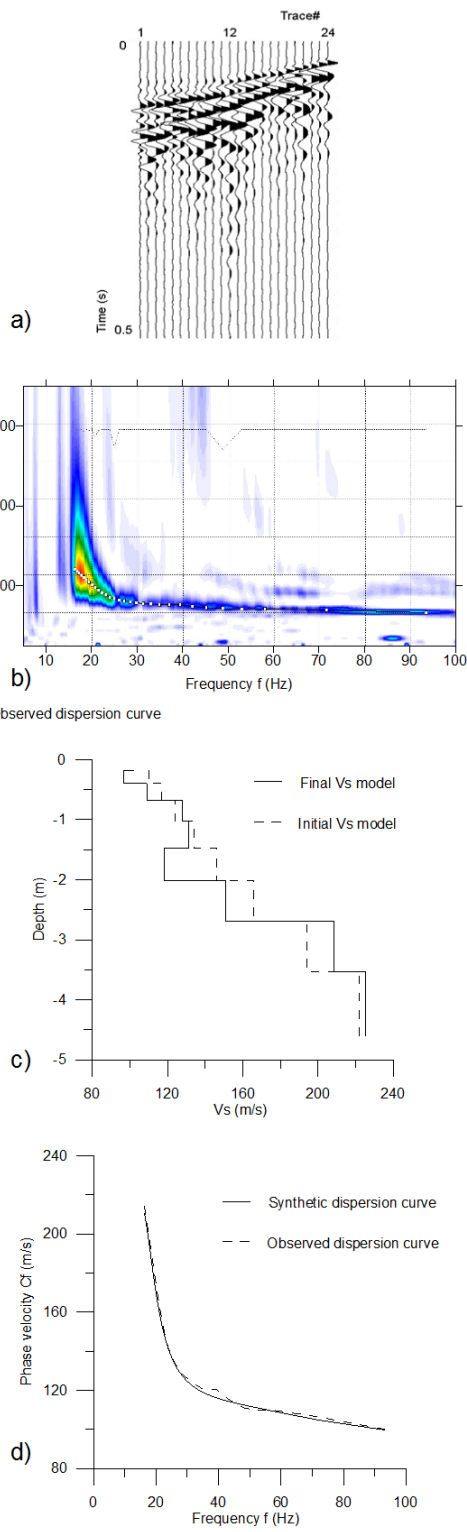


hal-00658933, version 1 - 11 Jan 2012

801

802

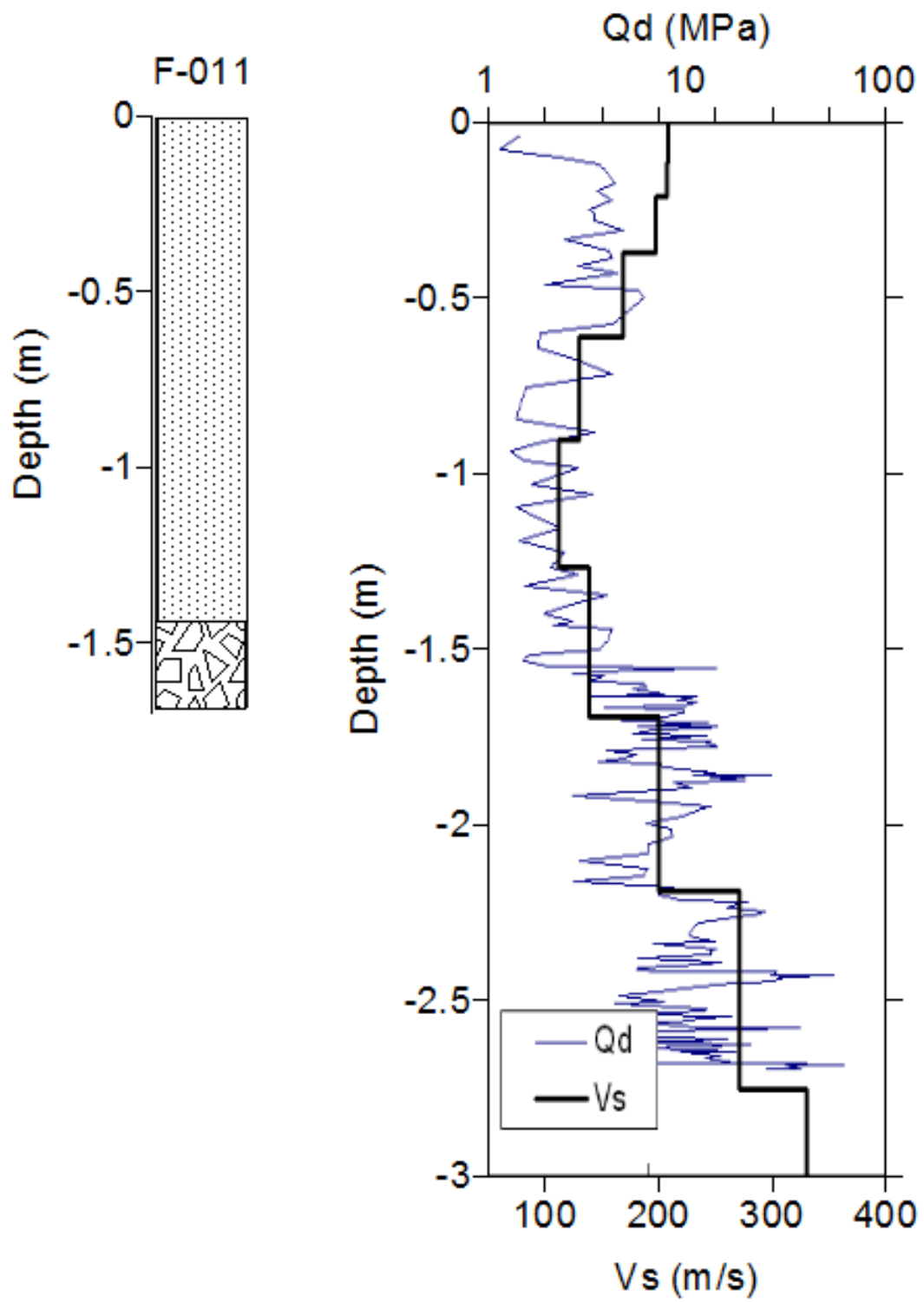
803 Figure 5



804



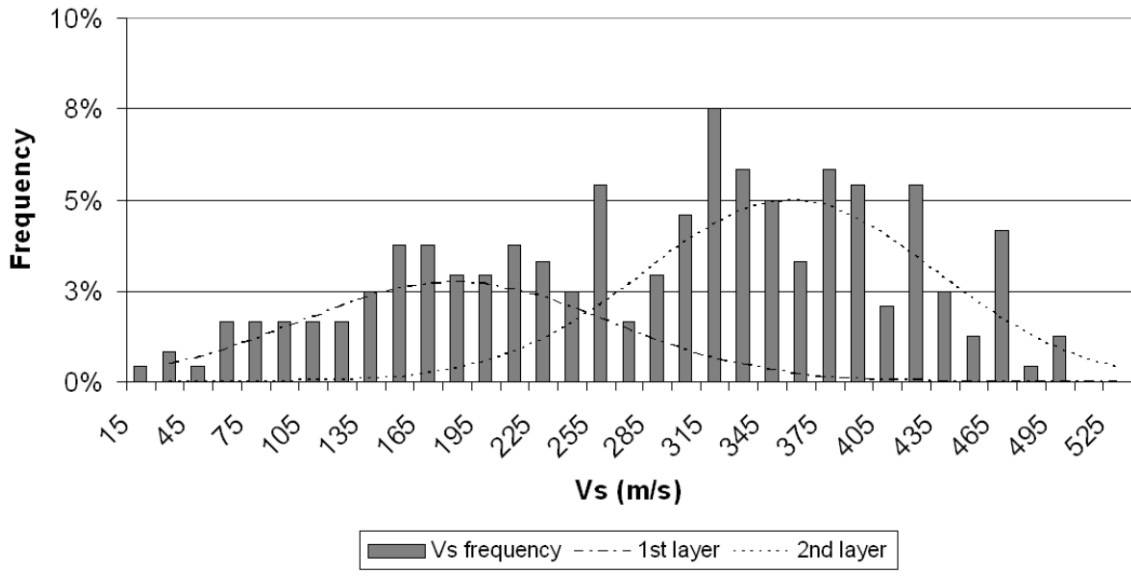
806 Figure 6



807

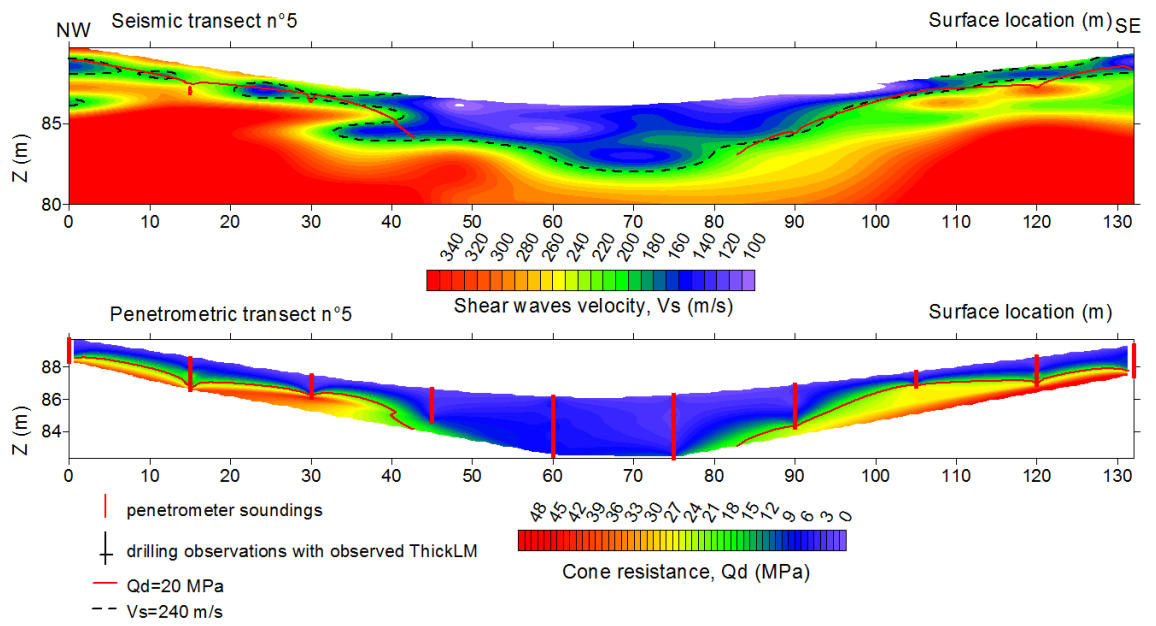
808

809 Figure 7



810  
811

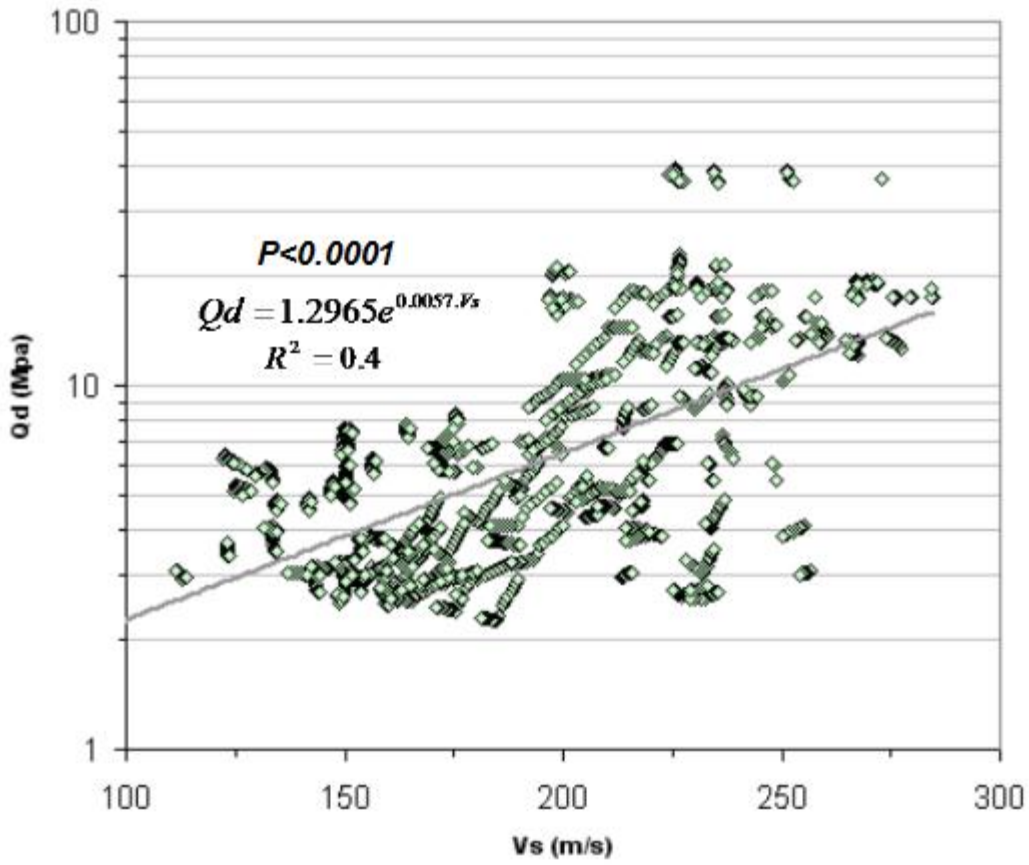
812 Figure 8



813

814

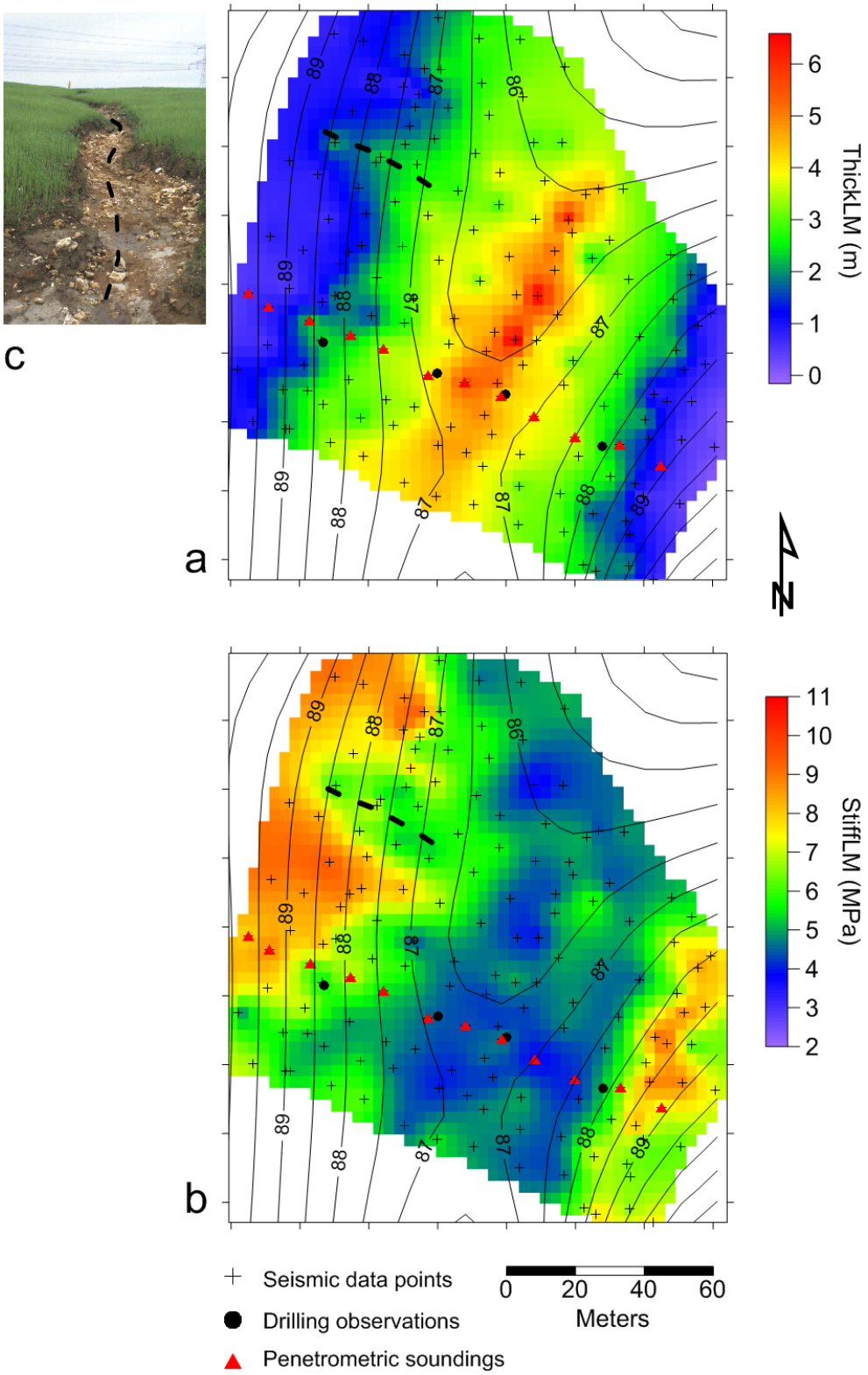
815 Figure 9



816

817

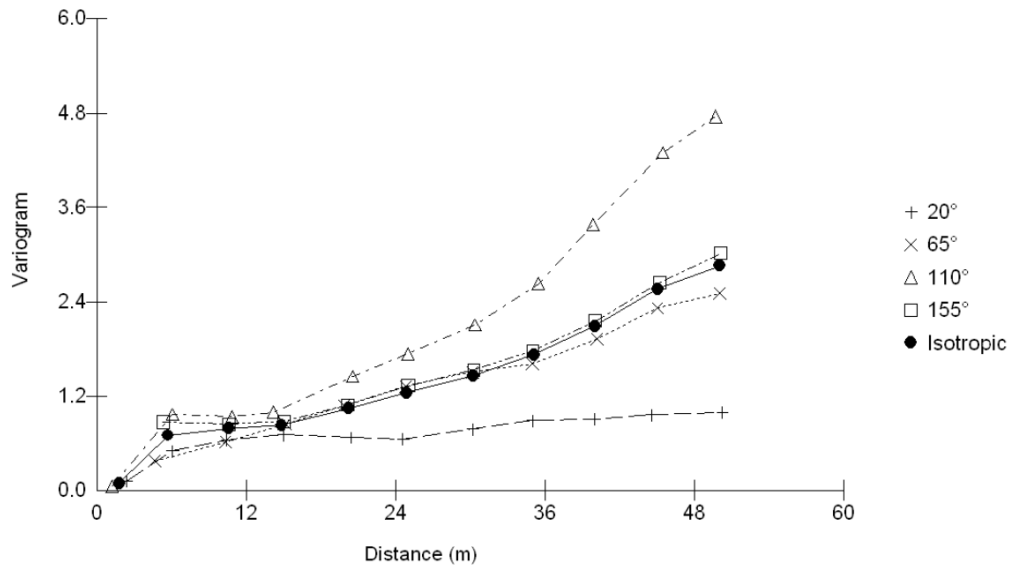
818 Figure 10



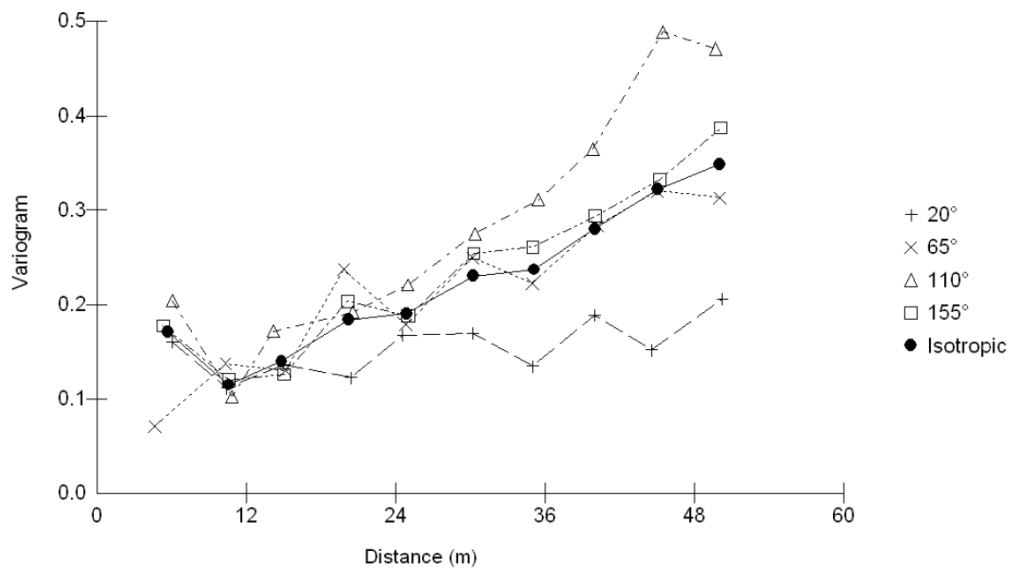
819



821 Figure 11



a

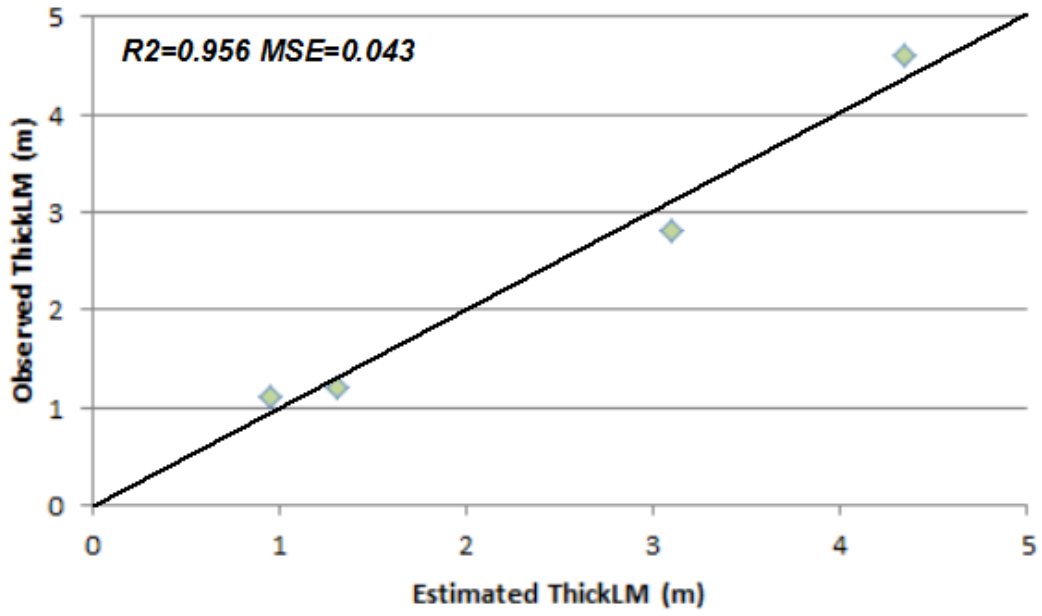


b

822

823

824 Figure 12



825